OPEN ACCESS

Applied Physics Express **10**, 122201 (2017)

https://doi.org/**10.7567/APEX.10.122201**

Switchable subwavelength plasmonic structures with phase-change materials for reflection-type active metasurfaces in the visible region

Chi-Young Hwang[1*], Seung-Yeol Lee[2], Yong-Hae Kim[1], Tae-Youb Kim[1], Gi Heon Kim[1], Jong-Heon Yang[1], Jae-Eun Pi[1], Ji Hun Choi[1], Kyunghee Choi[1], Hee-Ok Kim[1], and Chi-Sun Hwang[1*]

[1]*Reality Display Device Research Group, Electronics and Telecommunications Research Institute, Daejeon 34129, Republic of Korea*
[2]*Integrated Plasmonics and Optical Device Laboratory, School of Electronics Engineering, Kyungpook National University, Daegu 41566, Republic of Korea*

*E-mail: cyhwang@etri.re.kr; hwang-cs@etri.re.kr

Received August 5, 2017; accepted October 16, 2017; published online November 2, 2017

In this work, a switchable plasmonic structure is proposed for reflection-type spatial light modulation in the visible range with subwavelength resolution. This structure is based on a metallic grating in which each resonant cavity couples the incident light into a gap surface plasmon mode and then reflects the light modulated in the cavity. By incorporating an ultrathin layer of the phase-change material $Ge_2Sb_2Te_5$ at the entrance of the cavity, the optical modulation characteristic of the structure can be switched between two modes. Numerical investigations are conducted to verify the proposed structure, with the focused analysis of two common types of binary modulations: amplitude-only and phase-only modulations.
© 2017 The Japan Society of Applied Physics

Metasurfaces are the two-dimensional counterpart of metamaterials that consist of an array of subwavelength-scale optical antennas or resonators made of either plasmonic or dielectric materials.[1)] Because of their ability to alter various properties of light at a subwavelength spatial resolution, metasurfaces have been considered as a promising framework for high-performance diffractive optics for applications such as ultrathin, flat optical components[2–9)] and three-dimensional holographic displays.[10–14)] The wavefront manipulation at the subwavelength scale has an advantage in that the modulated light can be diffracted at large angles and is, therefore, free from unwanted diffraction orders.[15)]

The field of metasurfaces is continuously progressing, primarily to achieve high efficiency,[13,15)] obtain complex modulation schemes (independent/simultaneous phase and amplitude modulations),[10,16)] with large modulation depth and active modulation techniques.[17–26)] One of the most challenging techniques is the development of active modulation techniques for dynamic applications. Over the last few years, there have been pioneering contributions to introduce tunable optical properties to various metasurface configurations using materials such as graphene,[17–19)] indium tin oxide (ITO),[20–22)] and phase-change materials (PCMs).[23–27)]

The compound $Ge_2Sb_2Te_5$ (GST), a chalcogenide, is considered as one of the most useful PCMs having a decent thermal stability and a large number of phase transition cycles,[23–27)] hence making it suitable for application in active metasurface devices. The phase of GST can be optically (or electrically) switched between amorphous and crystalline, thereby dynamically tuning its optical properties. In the present work, although we confine our analysis to the two extreme states of GST, intermediate states with partial crystallization can also be achieved.[24)] These intermediate states can be used for multilevel gray-scale light modulation with increased depth as compared with that of binary modulation.

In this paper, we propose a switchable plasmonic light modulation structure with an ultrathin layer of GST. The proposed structure is capable of having a subwavelength pixel pitch, making it suitable for reflection-type active metasurfaces working in the entire visible range. In addition, the optical properties of the structure can be readily engineered by tailoring the structural dimensions of the resonant cavity. Comprehensive numerical simulations were conducted to analyze the performance of the structure.

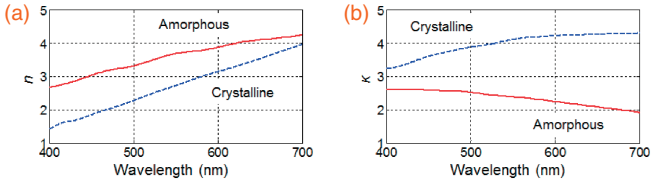

Fig. 1. (a) Refractive indices and (b) extinction coefficients of GST in amorphous and crystalline states at visible wavelengths.

Figure 1 shows the optical constants of GST in the amorphous and crystalline states experimentally obtained from ellipsometric measurements. In our GST sample preparation, the direct current sputtering method was used for the deposition of an amorphous GST thin film, and the deposited sample was crystallized by annealing at 300 °C for 2 h. As shown in the plots, when the amorphous GST is crystallized, the refractive index decreases while the extinction coefficient increases to a considerable level. Thus, despite the refractive index tunability being desirable, it is not recommended to use a large amount of GST in the light modulation structure because of its optically lossy nature at visible wavelengths. With all these considerations, it is reasonable to apply a minimum amount of GST at the crucial part of the structure to induce optical response switching.

The unit cell of the proposed structure, which extended infinitely along the *y*-axis, as illustrated in Fig. 2(a), is basically a subwavelength metallic grating[28–30)] whose fundamental period is 200 nm. As shown in the figure, two layers of silicon nitride (Si_3N_4) and GST are stacked within the aluminum (Al) slit cavity. For an array of these structures, the state of the GST layer embedded in each unit cell can be

Content from this work may be used under the terms of the Creative Commons Attribution 4.0 license. Any further distribution of this work must maintain attribution to the author(s) and the title of the work, journal citation and DOI.

© 2017 The Japan Society of Applied Physics

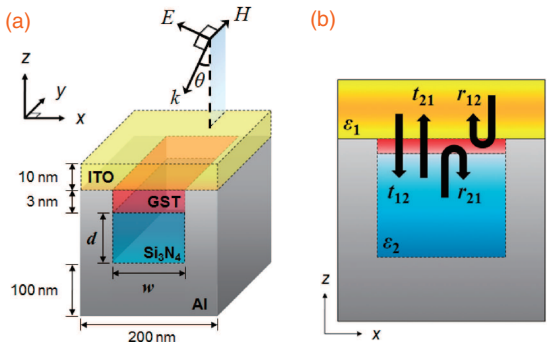

Fig. 2. (a) Schematic illustration of the unit cell structure for active modulation of visible light. (b) Transmission and reflection coefficients at the interface between the cavity and encapsulating ITO layer, assuming an infinitely thin GST layer.

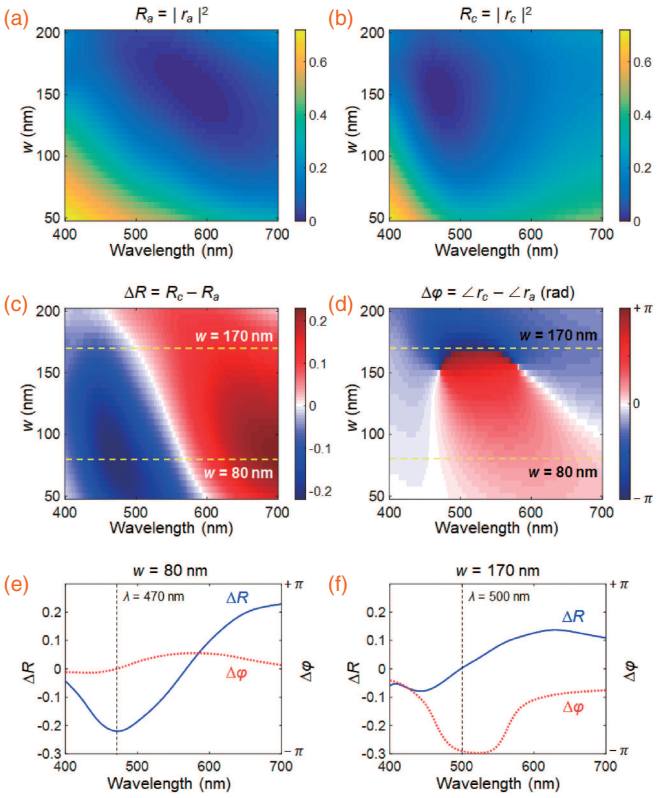

Fig. 3. Spectral reflectance maps with respect to the cavity width when GST is in (a) amorphous and (b) crystalline states, where r_a and r_c indicate the respective reflection coefficients for the configuration of periodically arranged unit cells. Maps for spectral (c) reflectance and (d) phase differences between the two light modulation modes for varying cavity width. (e) and (f) show spectral reflectance and phase differences for $w = 80$ and 170 nm, respectively. In all cases, normally incident TM plane waves are assumed, and the cavity depth is $d = 40$ nm.

reconfigured using the laser writing technique with patterned metal masks.[26] The structure is encapsulated with an ITO layer to protect the GST layer from oxidation and to confine the thermal energy within the GST layer for an effective phase change. In addition, the ITO thin film can be used as an electrical resistive heating element, potentially inducing the current-driven electrical phase switching of the GST layer.[26] The width and depth of the cavity, indicated as w and d, respectively, are variables that determine the optical response of the structure. We define the cavity depth d as the thickness of the Si_3N_4 layer, and the thicknesses of the ITO and GST layers are fixed at 10 and 3 nm, respectively. The thickness of the aluminum substrate is 100 nm, which is sufficient to assume zero transmission. The optical constants of the ITO and Al layers were measured experimentally by the same method as that used for the GST layer, and Si_3N_4 is assumed to be a lossless dielectric with refractive index 2. The coherent, monochromatic transverse magnetic (TM) plane wave is incident on the structure at an angle θ, with the magnetic field aligned parallel to the y-axis to excite the gap surface plasmon (GSP) modes in the cavity. Herein, E and H represent the electric and magnetic fields, respectively, and k indicates the wavenumber defined as $k = 2\pi/\lambda$, where λ is the wavelength of light.

The functional mechanism of the proposed structure can be intuitively understood from the description shown in Fig. 2(b), which relies on an assumption that the thickness of the GST layer is infinitely small, and hence, the effect caused by the internal reflections in the layer is negligible. Accordingly, it can be regarded that the GST layer simply alters the transmission and reflection coefficients t_{12}, t_{21}, r_{12}, and r_{21} at the interface between ITO and the dielectric medium, thereby switching the degree of light coupling and the resonance condition of the cavity.

In order to investigate the optical properties of the proposed structure, numerical simulations based on the transfer-matrix method were performed with the periodic boundary condition along the x-axis. Figures 3(a) and 3(b) show the spectral reflectance maps for the cavity width varying from 50 to 200 nm, with a fixed cavity depth of 40 nm. These maps clearly show the blue shift in the resonance wavelength of the structure with the phase transition of GST from amorphous to crystalline. The resonance condition where maximum absorption occurs can be expressed as

$$2k_{GSP}d + \varphi_u + \varphi_l = 2\pi m, \quad (1)$$

where k_{GSP} is the propagation constant of the GSP in the cavity, φ_u and φ_l indicate phase shifts due to the reflections at the upper and lower boundary interfaces of the cavity, respectively, and m is an integer that represents the resonance order.

In our model, the tunable shift in the resonance condition results from the change in φ_u in Eq. (1), which is the same as the argument of r_{21} ($\angle r_{21}$) in Fig. 2(b). This characteristic can be exploited for the amplitude and phase modulations, as shown in Figs. 3(c) and 3(d), revealing contrasts in modulated amplitude and phase between the two modulation modes. By selecting a suitable width from the map, we can determine the modulation function at a specific operating wavelength.

In particular, we study two different methods of amplitude-only and phase-only modulations by adopting the conditions of $w = 80$ and 170 nm as indicated by dotted lines in Figs. 3(c) and 3(d), respectively. The spectral profile for the amplitude-only modulation ($w = 80$ nm) is shown in Fig. 3(e). In this case, at a wavelength of 470 nm, the change in reflectance above 20% can be obtained, whereas there is near-zero phase contrast. On the other hand, for the case of the phase-only modulation ($w = 170$ nm) shown in Fig. 3(f), a nearly π-phase difference is achieved at a wavelength of 500 nm, having approximately the same reflectance.

The reflectance and phase contrast between the two modulation modes discussed in Figs. 3(e) and 3(f) can be

© 2017 The Japan Society of Applied Physics

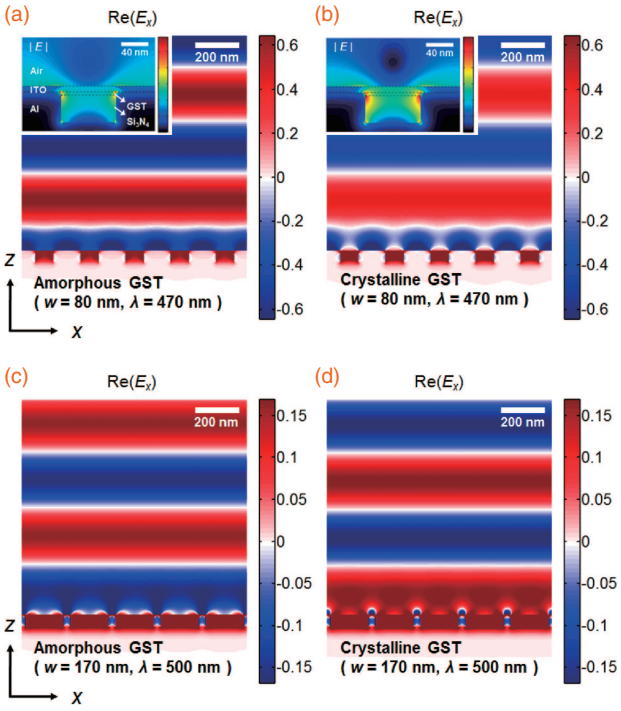

Fig. 4. Profiles of x-components of the electric fields that manifest the reflected wavefronts for (a) amorphous and (b) crystalline GST when $\lambda = 470$ nm, $d = 40$ nm, and $w = 80$ nm. The insets show the magnitude distributions of the electric fields in the unit cell. The field profiles for the two modulation modes when $\lambda = 500$ nm, $d = 40$ nm, and $w = 170$ nm are shown in (c) and (d). The calculation domain includes five elements out of an infinite array of unit cells, and the colormaps are appropriately normalized to clearly compare the relative magnitudes of the reflected fields.

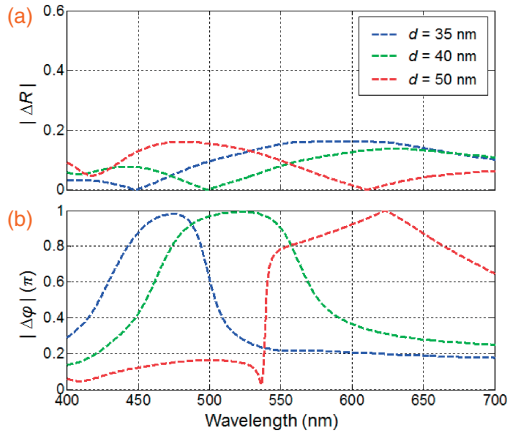

Fig. 5. Magnitudes of spectral (a) reflectance and (b) phase differences between two light modulation modes of the proposed structure for three different cavity depths $d = 35$, 40, and 50 nm, with the shared condition of $w = 170$ nm.

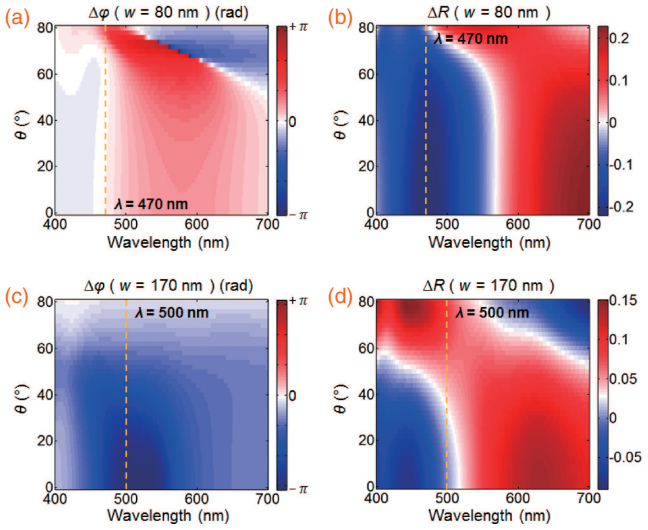

Fig. 6. Spectral (a) phase and (b) reflectance difference maps in the case of $w = 80$ nm (amplitude-only modulation at $\lambda = 470$ nm) with respect to the incidence angle up to 80° for TM polarization. Corresponding maps for $w = 170$ nm (phase-only modulation at $\lambda = 500$ nm) are shown in (c) and (d), respectively. For both cases, the cavity depth is $d = 40$ nm.

visually confirmed by calculating the electric field profiles. Figures 4(a) and 4(b) show the x-components of the electric fields reflected from the structure for two different modulation modes when $d = 40$ nm, $w = 80$ nm, and $\lambda = 470$ nm. As expected, the two profiles show almost no difference in their phase but a notable contrast in their amplitude. The corresponding reflectances are calculated as 41.5 and 19.5%, respectively. The difference in reflectance is attributed to the field enhancement on both sides of the cavity for the crystalline state, as can be found by comparing the field magnitude distributions in Figs. 4(a) and 4(b). In these structures, the reflectance decreases when the GSP modes become strongly confined within the cavity, resulting in an increased light absorption. The x-components of the electric fields reflected from the structure in two modes for $d = 40$ nm, $w = 170$ nm, and $\lambda = 500$ nm are shown in Figs. 4(c) and 4(d). By comparing the two profiles, we can see that the two modulated fields are nearly π out-of-phase while their amplitudes are almost the same.

For the utilization of the proposed structure across the whole visible spectrum, it is desirable for the operating wavelength to be tuned at will. Since the resonance wavelength can be shifted by changing the depth of the cavity, the same scheme can also be applied to the case of the operating wavelength. Figure 5 shows the spectral reflectance and phase differences between two modes for three cavity depths $d = 35$, 40, and 50 nm, with the cavity width of $w = 170$ nm in common, which is an appropriate condition for phase-only modulation as mentioned previously. For the three spectral curves in Fig. 5(b), the wavelengths where the phase difference is nearly π are calculated as visible lights of red, green, and blue colors. It is notable that the spectral response shifts to longer wavelengths as the cavity depth increases and vice versa. In addition, each spectral phase difference has a moderate bandwidth, which broadens as the operating wavelength redshifts. These properties can provide the opportunity to realize the color-selective diffraction that can be usefully adopted in applications such as full-color holographic imaging and displays using the spatial multiplexing technique.[12,14]

The tendency of variation in optical response depending on the incidence angle is important for the versatile use of the proposed structure. Figure 6 shows the spectral reflectance and phase difference maps with respect to the incidence angle θ. Here, the direction of the magnetic field is fixed to be aligned along the y-axis. For the cavity of $d = 40$ nm and $w = 80$ nm, which can perform amplitude-only modulation at a wavelength of 470 nm, the designed optical property is conserved up to around 60°, as shown in Figs. 6(a) and 6(b).

© 2017 The Japan Society of Applied Physics

On the other hand, for a larger cavity width of $w = 170\,\mathrm{nm}$ (phase-only modulation at $\lambda = 500\,\mathrm{nm}$), which is shown in Figs. 6(c) and 6(d), the corresponding structure retains its spectral profiles up to the incidence angle of 30°. This is not as robust as the former case, but still exhibits acceptable performance. The results demonstrate that the angular robustness, which is especially superior for smaller cavity widths, can be exploited for several purposes, such as beam-steering and holographic image generation, which often require obliquely incident input lights.

In conclusion, we have proposed a tunable plasmonic light modulation structure, which is based on a subwavelength metallic grating incorporated with GST acting as a PCM, working in the entire visible region. The modulation mode of the structure can be switched by thermally inducing the phase change in the ultrathin layer of GST, positioned at the entrance of the resonant cavity. In addition, the optical property can be easily tuned by appropriately selecting the design parameters, namely, the width and depth of the resonant cavity. The validity of the proposed structure was investigated by numerical simulations, with emphasis on the conditions of amplitude-only and phase-only modulations. Simulation results for the two cases demonstrate that over 20% switching in reflectance and nearly 180° switching in phase can be achieved. The proposed structure can be employed in a pixelated configuration that is electrically tunable by current pulses passing through the ITO layer, expanding its applicability in the field of advanced spatial light manipulation technology.

Acknowledgment This work was supported by "The Cross-Ministry Giga KOREA Project" grant funded by the Korea government (MSIT), (GK17D0100, Development of Telecommunications Terminal with Digital Holographic Table-top Display) and (GK17C0200, Development of Full-3D Mobile Display Terminal and Its Contents).

1) N. Yu and F. Capasso, Nat. Mater. **13**, 139 (2014).
2) N. Yu, P. Genevet, M. A. Kats, F. Aieta, J.-P. Tetienne, F. Capasso, and Z. Gaburro, Science **334**, 333 (2011).
3) N. Yu, F. Aieta, P. Genevet, M. A. Kats, Z. Gaburro, and F. Capasso, Nano Lett. **12**, 6328 (2012).
4) A. Pors, O. Albrektsen, I. P. Radko, and S. I. Bozhevolnyi, Sci. Rep. **3**, 2155 (2013).
5) D. Lin, P. Fan, E. Hasman, and M. L. Brongersma, Science **345**, 298 (2014).
6) F. Aieta, M. A. Kats, P. Genevet, and F. Capasso, Science **347**, 1342 (2015).
7) A. Arbabi, Y. Horie, M. Bagheri, and A. Faraon, Nat. Nanotechnol. **10**, 937 (2015).
8) M. Khorasaninejad, W. T. Chen, R. C. Devlin, J. Oh, A. Y. Zhu, and F. Capasso, Science **352**, 1190 (2016).
9) J. P. B. Mueller, N. A. Rubin, R. C. Devlin, B. Groever, and F. Capasso, Phys. Rev. Lett. **118**, 113901 (2017).
10) X. Ni, A. V. Kildishev, and V. M. Shalaev, Nat. Commun. **4**, 2807 (2013).
11) L. Huang, X. Chen, H. Mühlenbernd, H. Zhang, S. Chen, B. Bai, Q. Tan, G. Jin, K.-W. Cheah, C.-W. Qiu, J. Li, T. Zentgraf, and S. Zhang, Nat. Commun. **4**, 2808 (2013).
12) Y.-W. Huang, W. T. Chen, W.-Y. Tsai, P. C. Wu, C.-M. Wang, G. Sun, and D. P. Tsai, Nano Lett. **15**, 3122 (2015).
13) G. Zheng, H. Mühlenbernd, M. Kenney, G. Li, T. Zentgraf, and S. Zhang, Nat. Nanotechnol. **10**, 308 (2015).
14) W. Zhao, B. Liu, H. Jiang, J. Song, Y. Pei, and Y. Jiang, Opt. Lett. **41**, 147 (2016).
15) D. Sell, J. Yang, S. Doshay, R. Yang, and J. A. Fan, Nano Lett. **17**, 3752 (2017).
16) M. Kim, A. M. H. Wong, and G. V. Eleftheriades, Phys. Rev. X **4**, 041042 (2014).
17) Y. Yao, R. Shankar, M. A. Kats, Y. Song, J. Kong, M. Lončar, and F. Capasso, Nano Lett. **14**, 6526 (2014).
18) N. Dabidian, S. Dutta-Gupta, I. Kholmanov, K. Lai, F. Lu, J. Lee, M. Jin, S. Trendafilov, A. Khanikaev, B. Fallahazad, E. Tutuc, M. A. Belkin, and G. Shvets, Nano Lett. **16**, 3607 (2016).
19) M. C. Sherrott, P. W. C. Hon, K. T. Fountaine, J. C. Garcia, S. M. Ponti, V. W. Brar, L. A. Sweatlock, and H. A. Atwater, Nano Lett. **17**, 3027 (2017).
20) Y.-W. Huang, H. W. H. Lee, R. Sokhoyan, R. A. Pala, K. Thyagarajan, S. Han, D. P. Tsai, and H. A. Atwater, Nano Lett. **16**, 5319 (2016).
21) J. Park, J.-H. Kang, S. J. Kim, X. Liu, and M. L. Brongersma, Nano Lett. **17**, 407 (2017).
22) S. J. Kim and M. L. Brongersma, Opt. Lett. **42**, 5 (2017).
23) Y. Chen, X. Li, Y. Sonnefraud, A. I. Fernández-Domínguez, X. Luo, M. Hong, and S. A. Maier, Sci. Rep. **5**, 8660 (2015).
24) Q. Wang, E. T. F. Rogers, B. Gholipour, C.-M. Wang, G. Yuan, J. Teng, and N. I. Zheludev, Nat. Photonics **10**, 60 (2016).
25) A. Karvounis, B. Gholipour, K. F. MacDonald, and N. I. Zheludev, Appl. Phys. Lett. **109**, 051103 (2016).
26) S.-Y. Lee, Y.-H. Kim, S.-M. Cho, G. H. Kim, T.-Y. Kim, H. Ryu, H. N. Kim, H. B. Kang, C.-Y. Hwang, and C.-S. Hwang, Sci. Rep. **7**, 41152 (2017).
27) M. Wuttig, H. Bhaskaran, and T. Taubner, Nat. Photonics **11**, 465 (2017).
28) J. S. White, G. Veronis, Z. Yu, E. S. Barnard, A. Chandran, S. Fan, and M. L. Brongersma, Opt. Lett. **34**, 686 (2009).
29) W. Zhou, K. Li, C. Song, P. Hao, M. Chi, M. Yu, and Y. Wu, Opt. Express **23**, A413 (2015).
30) C.-Y. Hwang, Y. Yi, and C.-G. Choi, Opt. Lett. **41**, 990 (2016).

© 2017 The Japan Society of Applied Physics